High-temperature transformation in AlMn(Si) quasi-crystals

1989 J. Phys.: Condens. Matter 1 3421

(http://iopscience.iop.org/0953-8984/1/22/004)

J. Phys.: Condens. Matter 1 (1989) 3421–3432. Printed in the UK

High-temperature transformation in AlMn(Si) quasi-crystals

C Berger†, F Cyrot-Lackmann†, J Devenyi†, G Fourcaudot†, P Germi‡, J C Grieco† and D Pavuna†§

† Laboratoire d'étude des propriétés électroniques des solides, CNRS, 25 avenue des Martyrs, BP 166, 38042 Grenoble Cedex, France

‡ Laboratoire de cristallographie, CNRS, 25 avenue des Martyrs, BP 166, 38042 Grenoble Cedex, France

Received 11 April 1988, in final form 8 December 1988

Abstract. Transformations of the quasi-crystalline icosahedral phases formed in the melt-spun AlMn(Si) alloys $Al_{90}Mn_{10}$, $Al_{86}Mn_{14}$ and $Al_{75}Mn_{20}Si_5$ have been studied at high temperatures (300–1000 K) by combined measurements of resistivity, differential scanning calorimetry and x-ray diffraction. In $Al_{86}Mn_{14}$ a direct crystallisation of both the icosahedral phase and the intergranular AlMn solid solution into o-Al_6Mn is observed. It is preceded by a 'relaxation' phenomenon, as seen by the DSC curve. The amplitude and temperature dependence of resistivity are well understood by taking into account the different phase contributions to resistivity during the transformation. The same analysis accounts for the measurements of the $Al_{90}Mn_{10}$ sample. The crystallisation of $Al_{75}Mn_{20}Si_5$ into β-Al_9Mn_3Si is more complex and involves several intermediate crystalline phases, in particular the α-$Al_{12}Mn_3Si$. Finally, the better stability of the icosahedral phase in $Al_{75}Mn_{20}Si_5$ (~700 K) compared with AlMn samples (~600 K) suggests possible structural and electronic differences between the two icosahedral phases.

1. Introduction

The discovery of a long-range icosahedral order in melt-spun AlMn alloys [1] has raised many questions concerning the atomic structure of these new materials and the consequences of this structure in relation to the physical properties [2]. For instance, electronic properties of AlMn(Si) icosahedral phases (i-phases) have recently been investigated and are now well understood by the existence of a virtual bound states type electronic density of states, which is related to a tendency of Mn first-neighbour exclusion in the icosahedral phase [3, 4].

In order to elucidate the quasi-crystalline (QC) structures, the crystallisation study of these metastable phases may provide useful information. Previous studies have been devoted to QC crystallisation [5–11], but few of them associate direct experimental evidence for structural transformations (x-ray diffraction, electron microscopic examination, differential scanning calorimetry experiments (DSC)) and measurements of electronic properties. Furthermore, only little work [9] has been performed on ternary AlMnSi alloys although these may lead to almost pure icosahedral phases.

§ Present address: EPFL/Physics department, PHB Ecublens, CH-1015 Lausanne, Switzerland.

0953-8984/89/223421 + 12 $02.50

The purpose of the present paper is to study by complementary measurements of resistivity, DSC and x-ray diffraction the high-temperature (300–1000 K) behaviour of the AlMn(Si) i-phase formed in the melt-spun $Al_{90}Mn_{10}$, $Al_{86}Mn_{14}$ and $Al_{75}Mn_{20}Si_5$ alloys. We first present our resistivity and DSC results during the crystallisation of $Al_{75}Mn_{20}Si_5$, $Al_{86}Mn_{14}$ and $Al_{90}Mn_{10}$, respectively, into the compounds β-Al_9Mn_3Si, o-Al_6Mn and a mixture of Al_6Mn and Al. We then analyse the resistivity behaviour of the AlMn samples within a two-phase model. With this analysis, associated with the study of the DSC and x-ray patterns during structural transformations, we propose a description of the AlMn sample crystallisation. Finally, the complex transformations in the $Al_{75}Mn_{20}Si_5$ sample and the subsequent broad $\rho(T)$ variations are presented.

2. As-quenched samples: production and structural studies

We prepared a series of metallic ribbons using an improved melt-spinning technique [12] in the composition range $Al_{100-x}Mn_x$ ($x = 3, 10, 14, 20$ at.% Mn) and $Al_{80-y}Mn_{20}Si_y$ ($y = 1, 2, 5$ at.% Si). We thus obtained brittle ribbons ~20 μm thick. We quenched with moderate roller speed (30–40 m s^{-1}) in order to accommodate convenient geometrical shapes for resistivity measurements and the presence of the i-phase.

All the samples were studied by x-ray powder diffraction (Cu Kα radiation) and transmission electron microscopy (Philips EM400T). The icosahedral phase was observed in all samples by both techniques. Diffraction patterns of these alloys are given in figure 1; we see the sharp peaks of the i-phase (indexed in Cahn's notation [13]) and of the decagonal 'T' phase, together with FCC Al peaks.

(i) The Al peaks of $Al_{90}Mn_{10}$ and $Al_{86}Mn_{14}$ are slightly shifted as compared with pure Al; this indicates a solid solution of Mn in Al of about 3 at.% [14], which is confirmed by measurements of a ribbon of $Al_{97}Mn_3$ solid solution.

(ii) The volume fractions of the phases present in the samples are schematically drawn in figure 2. For the two-phase samples, the values are estimated from electron microscopic images (giving an upper limit due to variations in grain size in the section of the ribbon), and from a simple calculation by sharing Mn atoms between the two coexisting phases (assuming a concentration of 20 ± 2 at.% Mn in the i-phase [15, 8]). Both estimates give roughly the same volume fraction of ~50 vol% for $Al_{90}Mn_{10}$ and ~70 vol% for $Al_{86}Mn_{14}$.

(iii) $Al_{75}Mn_{20}Si_5$ consists almost entirely of the i-phase; the substitution of a few per cent of Al by Si indeed avoids the formation of the decagonal 'T' phase in the more concentrated alloy (20 at.% Mn). As seen in figure 1, at least 2 at.% Si is required to stabilise the i-phase with the quenching rate we used.

In the following we focus our attention on samples containing only the i-phase (and AlMn solid solution), with a special emphasis on the samples which contain the highest volume fraction of i-phase ($Al_{75}Mn_{20}Si_5$ and $Al_{86}Mn_{14}$). The behaviour of the 'T' phase will be studied elsewhere.

3. Experimental results

3.1. Resistivity behaviour and DSC spectra

Differential scanning calorimetric measurements were carried out in a Perkin–Elmer DSC 2 with varying scanning rates: 5, 10, 20 and 40 K min^{-1}. The electrical resistivity

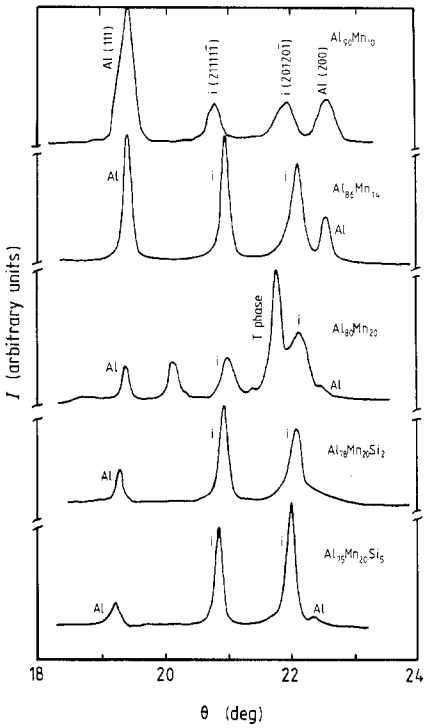

Figure 1. X-ray diffraction patterns of $Al_{90}Mn_{10}$, $Al_{86}Mn_{14}$, $Al_{80}Mn_{20}$, $Al_{78}Mn_{20}Si_2$, and $Al_{75}Mn_{20}Si_5$ as-quenched alloys (Cu Kα radiation).

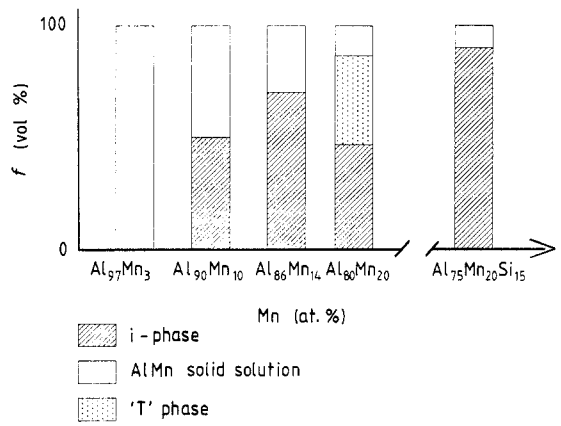

Figure 2. Schematic presentation of various phases present in as-quenched AlMn(Si) samples.

was measured by using the standard DC four-probe technique from 300 to 1000 K in a low-inertia, regulated oven, with the same heating rates of 5–40 K min^{-1}. The electrical contacts were made by flat copper wires pressed onto the sample. The low-temperature resistivities had previously been measured [3] in the temperature range 0.3–300 K with conventional ^{4}He and ^{3}He cryostats.

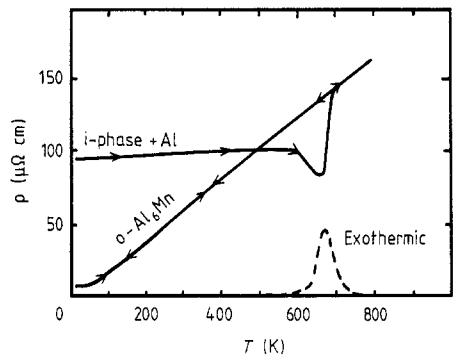

Figure 3. Temperature dependence of resistivity (0.3 K–800 K) and DSC measurements ($T > 500$ K) of $Al_{86}Mn_{14}$ (scanning rate for the irreversible part ($T > 300$ K) 10 K min^{-1}).

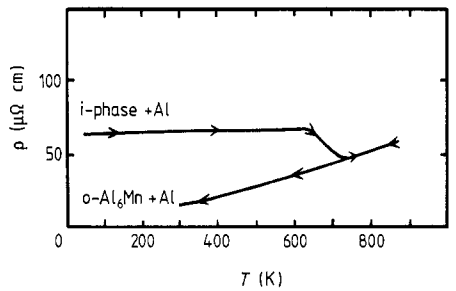

Figure 4. Temperature dependence of resistivity of $Al_{90}Mn_{10}$ (10 K min^{-1}).

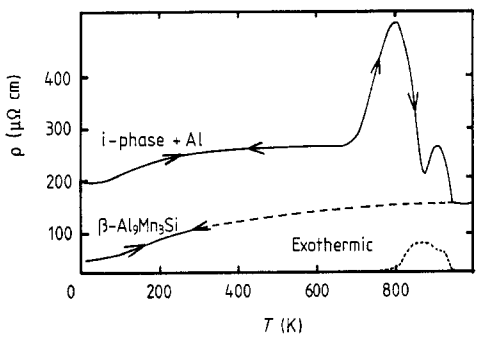

Figure 5. Temperature dependence of resistivity and DSC of $Al_{75}Mn_{20}Si_5$ (10 K min^{-1}).

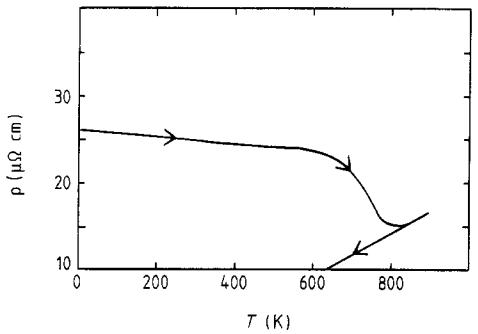

Figure 6. Temperature dependence of resistivity of $Al_{97}Mn_3$ (10 K min^{-1}).

X-ray diffraction was performed also on partially annealed samples: the ribbons were heated (10 K min^{-1}) up to the chosen temperature and immediately quenched in water to preserve their annealed structures.

Figures 3, 4 and 5 show the temperature dependence of resistivity (0.3–1000 K) for $Al_{90}Mn_{10}$, $Al_{86}Mn_{14}$ and $Al_{75}Mn_{20}Si_5$. The DSC spectra of $Al_{86}Mn_{14}$ and $Al_{75}Mn_{20}Si_5$ obtained at the same scanning rate (10 K min^{-1}) are also plotted for $T > 500$ K. We can thus follow the structural transformations of the samples, as seen by the irreversible variation in resistivity and the exothermic DSC behaviour.

The crystallised samples were studied by x-ray diffraction. $Al_{90}Mn_{10}$ transforms into a mixture of the orthorhombic compound o-Al_6Mn and Al; each of the $Al_{86}Mn_{14}$ and $Al_{75}Mn_{20}Si_5$ samples crystallised into an almost single phase: o-Al_6Mn and hexagonal β-Al_9Mn_3Si, respectively.

We first analyse the results for the as-quenched samples. We note in figures 3–5 that the value of resistivity ρ_{4K} is greatly increased in the samples containing the i-phase as compared with the corresponding crystalline phases (table 1), and is of the same order of magnitude as the resistivities usually measured in amorphous samples. Moreover, below the i-phase transformation ($T < 600$ K) the temperature coefficients $\alpha = (1/\rho)\Delta\rho/\Delta T$ (table 1) are much smaller than for the recrystallised samples, which exhibit

Table 1. Residual resistivity and temperature coefficients for as-quenched and annealed samples.

Sample	Structure	ρ_0 ($\mu\Omega$ cm)	$(1/\rho_0)\,\Delta\rho/\Delta T$ (K^{-1})
$Al_{97}Mn_3$	solid solution	25 ± 1	1.0×10^{-4}
$Al_{90}Mn_{10}$	i-phase + **Al**Mn	65 ± 5	3.5×10^{-5}
	o-Al_6**Mn** + **Al**Mn	—	4.5×10^{-2}
$Al_{86}Mn_{14}$	i-phase + **Al**Mn	100 ± 10	1.0×10^{-4}
	o-Al_6**Mn**	5 ± 5	6.0×10^{-2}
$Al_{75}Mn_{20}Si_5$	i-phase + **Al**	200 ± 10	8.5×10^{-4}
	β-Al_9Mn_3Si	50 ± 5	3.7×10^{-1}

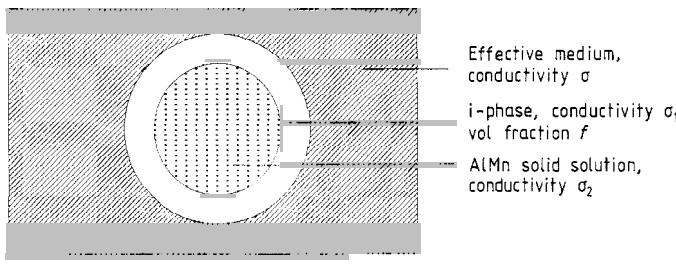

Figure 7. Geometry of the domains (i-phase and AlMn solid solution) in the two-phase resistivity model for the AlMn samples.

linear $\rho(T)$ variations denoting a metallic behaviour. These low-temperature coefficients are related to the high resistivity values according to the well known Mooij correlation.

In the AlMn case, we estimated ρ_{QC} for the i-phase from the two-phase sample data using a two-phase resistivity model. We also studied the resistivity behaviour of an $Al_{97}Mn_3$ solid solution, which is roughly the composition of the intergranular phase in $Al_{86}Mn_{14}$ and in $Al_{90}Mn_{10}$.

The low residual resistivity (25 $\mu\Omega$ cm) of $Al_{97}Mn_3$ (figure 6) is similar to earlier results on **Al**Mn solid solutions [16]. Around 700 K, the rapid decrease in $\rho(T)$ corresponds to the precipitation from the solid solution. Below this structural transformation (<650 K), the negative temperature coefficient had previously been described by a spin fluctuation mechanism [17].

3.2. Two-phase resistivity model

Two-phase materials such as granular systems have been extensively studied; the resistivity data on these systems are usually analysed within models based on the effective medium approximation. The models differ essentially in the geometry of the phase domains. We chose here a geometry close to our electron microscopic observations, in which each phase 1 domain (here the i-phase in volumetric fraction f) is surrounded by a phase 2 (**Al**Mn solid solution in volume fraction $1 - f$), both embedded in an effective medium (figure 7).

Table 2. Parameters for the two-phase resistivity model calculation in $Al_{86}Mn_{14}$ and $Al_{90}Mn_{10}$: total resistivity ρ_0 ($\mu\Omega$ cm) of the sample; estimated volumetric fraction of the i-phase f_v (vol%); Mn concentration in the AlMn solid solution (at.% Mn); resistivity of the AlMn solid solution.

Sample	ρ_0 (sample) ($\mu\Omega$ cm)	f_v (i-phase) (vol %)	at.% Mn in AlMn	ρ_0 AlMn ($\mu\Omega$ cm)
$Al_{86}Mn_{14}$	100 ± 10	70 ± 10	3 ± 1	15–30
$Al_{90}Mn_{10}$	65 ± 5	45 ± 5	3 ± 1	15–30

The relation between the conductivities σ_1 and σ_2 of the respective phases is then written [18]:

$$\frac{\sigma - \sigma_1}{\sigma + 2\sigma_2} = (1 - f)\frac{\sigma_2 - \sigma_1}{\sigma_2 + 2\sigma_1}$$

σ being the total conductivity of the sample.

Using the experimental parameters of table 2, we estimate a resistivity ρ_{QC} for the i-phase in $Al_{86}Mn_{14}$ and in $Al_{90}Mn_{10}$ of the order 150–200 $\mu\Omega$ cm. A Landauer model [19] with spherical rather than concentric domains gives essentially the same result. We note that the resistivity for the i-phase is of the same order as the 200 $\mu\Omega$ cm resistivity measured in our other QC system, $Al_{75}Mn_{20}Si_5$, which is an almost pure i-phase. We also note that the i-phase resistivity must also vary little with temperature, in view of the weak temperature resistivity variations of the whole sample and of the intergranular AlMn solid solution.

4. AlMn: temperature variation of resistivity

We now analyse the temperature variation of the AlMn sample resistivities during the structural transformation ($T \geqslant 600$ K at a heating rate of 10 K min^{-1}). As presented in figure 3 for $Al_{86}Mn_{14}$, the minimum and the following sharp increase between 650 K and 740 K are irreversible phenomena. The position of the DSC peak indicates that the main crystallisation occurs in this temperature range. The resistivity curve then exhibits the linear reversible behaviour of the o-Al_6Mn compound. For $Al_{90}Mn_{10}$, as seen by the $\rho(T)$ variation, the transformation lies in the same temperature range, which is a good indication that a similar transformation occurs in both samples. For that reason, we first analyse the behaviour of the $Al_{86}Mn_{14}$ sample which contains the highest volume fraction of the i-phase, and next deal with the $Al_{90}Mn_{10}$ sample.

4.1. $Al_{86}Mn_{14}$: crystallisation into o-Al_6Mn

Up to 600 K the i-phase is stable, as shown by the reversible $\rho(T)$ curve and DSC spectrum of figure 3 and the x-ray diffraction patterns of figure 8. Neither change in the icosahedral domains nor grain growth are observed by electron microscopy.

Above 600 K, a gradual evolution of the DSC curve is observed below the peak, which was attributed to a relaxation phenomenon in the i-phase [5]. This exothermic contribution may also correspond to the onset of crystallisation (for an annealing up to

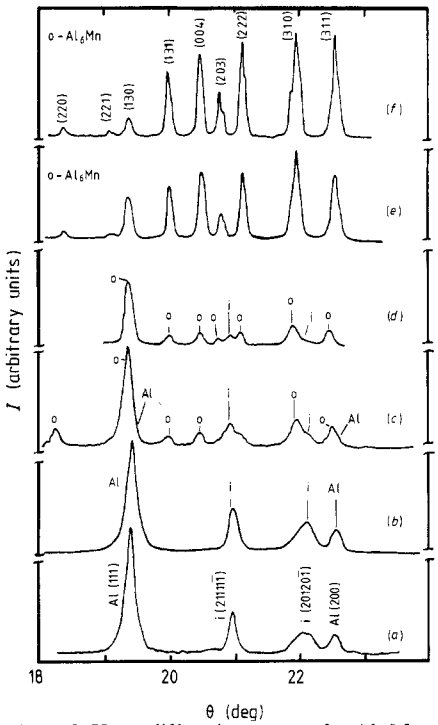

Figure 8. X-ray diffraction pattern for $Al_{86}Mn_{14}$: (*a*) as-quenched; annealed up to (*b*) 645 K, (*c*) 680 K, (*d*) 710 K, (*e*) 740 K, (*f*) 910 K. Annealing temperatures correspond to the curvature changes in $\rho(T)$ at a constant heating rate (10 K min^{-1}). The double $K\alpha_1$–$K\alpha_2$ radiation gives rise to a splitting of the x-ray diffraction peaks only for well crystallised phases (as in (*f*)).

645 K tiny deviations of the x-ray pattern are observed at the position of the intense o-Al_6Mn peaks).

At higher temperatures (650–750 K), the $Al_{86}Mn_{14}$ sample clearly crystallises into o-Al_6Mn, as observed by the x-ray patterns of figure 8. We point out that at the temperature of the resistivity minimum (685 K), the $Al_{86}Mn_{14}$ sample still contains an appreciable volume fraction of Al which decreases considerably from 710 K to 740 K. After annealing at 740 K, we observe only the o-Al_6Mn phase in both x-ray diffraction and electron microscopy investigations.

From these structural studies we conclude that a direct crystallisation of $Al_{86}Mn_{14}$ into o-Al_6Mn takes place. This is also shown by DSC experiments which exhibit a single exothermic peak. The total crystallisation enthalpy is measured by the DSC peak area: for a heating rate of 10 K min^{-1}, we find $\Delta H = 1.6$ kJ mol^{-1}, which is in the range of values published on these systems [5–8].

Moreover, we point out the correlation between the $\rho(T)$ and the DSC curves: their variations are both shifted to higher temperatures as the heating rate increases (5–40 K min^{-1}); the DSC peak position always corresponds to the sharp $\rho(T)$ increase (figure 9). From the DSC peak shift, we could estimate an effective activation energy Q for the transformation, by using the Kissinger plot [20]: $\ln(T_m^2/\Delta) = Q/k_B T_m$, where T_m is the temperature of the DSC peak maximum, and Δ is the heating rate. From this plot (see inset in figure 9) we estimate $Q = 1.7 \pm 0.2$ eV/atom, which again compares well with other published Q-values for quasi-crystalline samples.

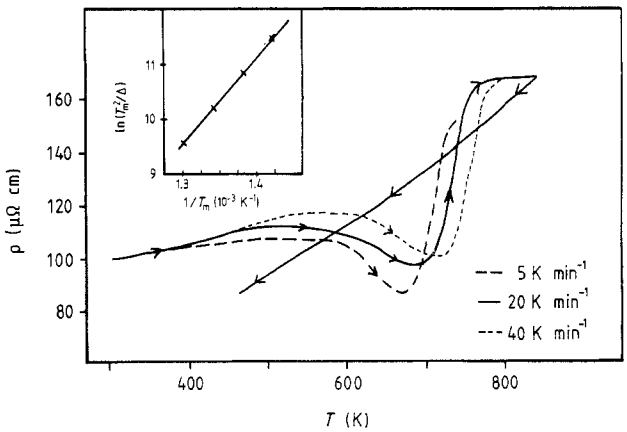

Figure 9. Variation with heating rate of the $\rho(T)$ curve for $Al_{86}Mn_{14}$. Inset, Kissinger plot for the DSC peak, Δ being the heating rate and T_m the temperature of the peak maximum.

These overall values for our DSC results show that, as for the crystallisation behaviour we wish to study here, our samples are quite similar to quasi-crystalline melt-spun samples produced in other laboratories, and present about the same degree of metastability.

4.2. *Resistivity analysis in $Al_{86}Mn_{14}$*

By measuring physical properties such as resistivity and DSC, we can distinguish two steps of crystallisation that are not seen by direct observations of the structures. The first one ($\sim 600\ K < T < \sim 630\ K$) corresponds to the slight exothermic prepeak in DSC measurements and is ascribed to a relaxation phenomenon [5]. The second step corresponds to the DSC peak itself and so to the main crystallisation of the entire sample ($630\ K < T < 740\ K$). We first study this second step.

The i-phase and the **Al**Mn solid solution contained in the as-quenched $Al_{86}Mn_{14}$ sample transform into the o-Al_6Mn compound. Since neither the **Al**Mn solid solution nor the i-phase have the o-Al_6Mn composition, the final crystallisation implies a diffusion of atomic species (Al into the i-phase or Mn out). However, since no crystallisation of intermediate phases is observed, atomic diffusion prior to crystallisation would imply an increase in Mn dissolved in the FCC solid solution. This cannot be energetically favourable, since the o-Al_6Mn phase is thermodynamically more stable than the i-phase, and therefore should co-exist in equilibrium with an FCC phase of lower rather than higher solute content. The system most probably reacts by a nucleation and growth mechanism of the o-Al_6Mn phase surrounding the QC grains (i.e., at the boundaries between the Al-rich and Mn-rich phases), as emphasised by [11]. The evolution of the x-ray peak intensities (§ 4.1) is also in agreement with a simultaneous transformation of the i-phase and of the **Al**Mn solid solution. Furthermore, as seen by the resistivity curve of figure 6 for an **Al**Mn solid solution containing 3 at.% Mn, the decomposition of the solid solution by precipitation starts around 630 K, i.e., at the beginning of the $Al_{86}Mn_{14}$ transformation (the onset of the DSC peak and the decrease in the $\rho(T)$ curve).

The resistivity behaviour is very sensitive to the overall transformation of the sample; during crystallisation the sample contains two phases of large resistivity ($\rho_{\text{i-phase}} = 150$–

200 $\mu\Omega$ cm and $\rho_{o\text{-}Al_6Mn} = 130\text{–}150\ \mu\Omega$ cm), and a low-resistivity phase ($\rho_{AlMn} < 25\ \mu\Omega$ cm). While the volume fraction of the solid solution decreases strongly (645–710 K), this low-resistivity phase thus contributes less and less to the total resistivity which consequently increases up to the high values and to the final single o-Al_6Mn value. However, as long as there remains an appreciable amount of Al-rich phase, which keeps the low-resistivity paths, the partial transformation of the i-phase into the o-Al_6Mn phase of lower resistivity leads to a decrease in the total resistivity. The presence of an intergranular low-resistivity solid solution in the temperature range 600–645 K, as seen by the intensity of the Al peaks in the $Al_{86}Mn_{14}$ x-ray diffraction, thus explains the $Al_{86}Mn_{14}$ $\rho(T)$ decrease in the temperature range 645–685 K. This $\rho(T)$ decrease may also be strengthened by a slight lowering in AlMn resistivity due to the beginning of precipitation from solid solution, but that alone cannot account for the 15% decrease in the total resistivity.

Before this step of total ribbon crystallisation ($T < 630$ K), the slight exothermic DSC pre-peak indicates that structural transformations of low-energy processes already occur in the sample for which no evidence is seen by either electron microscopy or x-ray diffraction; they may be relaxation phenomena as suggested by Chen [5], or reorganisation of disordered domains [21]. Both would lead to a decrease in the i-phase contribution to resistivity and thus also contribute to the initial $\rho(T)$ decrease.

The temperature resistivity variations are also sensitive to the state of crystallisation of o-Al_6Mn. Figure 10 presents the $\rho(T)$ behaviour of $Al_{86}Mn_{14}$ during thermal cyclings, immediately after the crystallisation into o-Al_6Mn. The slope $\Delta\rho/\Delta T$ remains almost identical after each cycle, while the resistivity amplitude slightly decreases. This is well understood by the grain coarsening, as observed by electron microscopy. After annealing at 740 K and at 900 K, the grain size indeed increases from an average of ~1000 Å to a few μm (figure 10). The variation in resistivity amplitude during grain coarsening is however rather small compared with the total 150 $\mu\Omega$ cm resistivity. This indicates that the grain boundaries of these highly resistive and already well crystallised systems have a relatively small influence on the total resistivity of the ribbon. For the icosahedral grains, spread over more than ~1000 Å and which have a similar order of magnitude of resistivity, this observation strengthens our crude estimate of i-phase resistivity in $Al_{86}Mn_{14}$, for which grain boundaries were not taken into account.

For $Al_{90}Mn_{10}$, the structural transformation can be described in the same way as the crystallisation of $Al_{86}Mn_{14}$. Because of the lower Mn content, $Al_{90}Mn_{10}$ crystallises into a mixture of o-Al_6Mn and Al. The resistivity behaviour is again explained by the contributions of a highly resistive i-phase and of a low-resistivity AlMn solid solution; but the presence of an Al phase even after sample transformation keeps the low-resistivity paths and thus avoids the $\rho(T)$ increase during crystallisation that was observed in $Al_{86}Mn_{14}$.

5. $Al_{75}Mn_{20}Si_5$ sample

We now present our results for resistivity, DSC and x-ray diffraction for an almost pure quasi-crystalline sample: $Al_{75}Mn_{20}Si_5$. The resistivity and DSC curves of figure 5 show that the transformation sequences are totally different from the AlMn samples. The first interesting feature is the improved stability of the AlMnSi i-phase as compared to the corresponding AlMn i-phase: the first noticeable resistivity variation starts around 700 K, as compared with 600 K in $Al_{86}Mn_{14}$. This has to be understood together with the

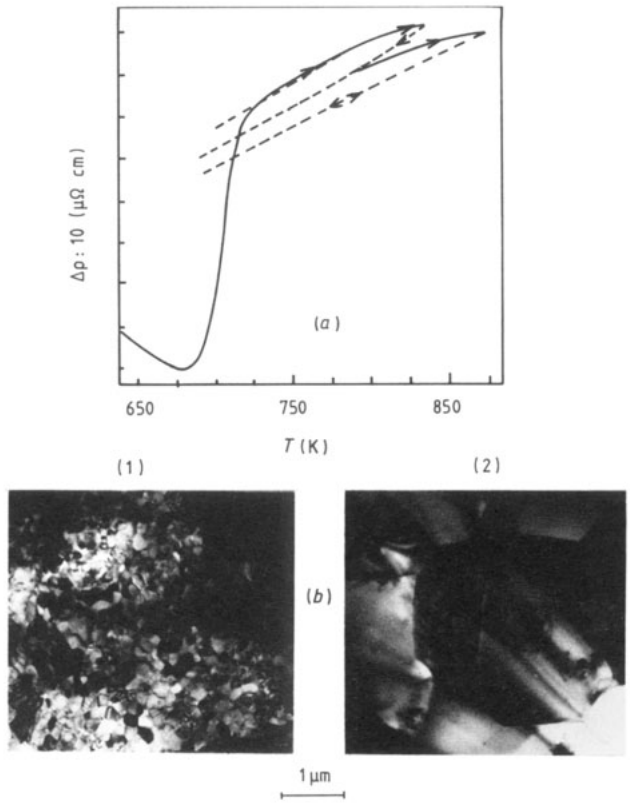

Figure 10. (*a*) High-temperature recyclings: resistivity for $Al_{86}Mn_{14}$ annealed into o-Al_6Mn. (*b*) Transmission electron images of o-Al_6Mn grain coarsening upon $Al_{86}Mn_{14}$ annealings up to: (1) 740 K, (2) 910 K.

fact that the addition of Si stabilises the i-phase during the elaboration process, since it avoids the decagonal 'T' phase formation (see § 2).

The $\rho(T)$ and DSC curves show complex behaviour: the resistivity reaches very high values, up to 500 $\mu\Omega$ cm, while the DSC spectrum reveals several structural transformations, with a wide exothermic peak over 800–900 K. These transformations are not easily analysed since no phase diagram is available in this concentration range. Analysis of the x-ray diffraction patterns of partially annealed samples (figure 11) reveals the continuous growth of the hexagonal β-Al_9Mn_3Si phase during annealing. Around 800 K, the high resistivity values obtained may indicate the presence of a very resistive phase; a ribbon annealed at 790 K indeed exhibits small additional peaks not yet indexed. They might correspond to AlMn phases but the complex structures of several AlMn phases in the compositional range 20–25 at.% Mn are not known at present. A possible 'T' phase growth is also under investigation. The second bump in $\rho(T)$ could be explained by the intermediate growth of the α-$Al_{12}Mn_3Si$ phase: we indeed observe the emergence and vanishing of the cubic α-$Al_{12}Mn_3Si$ phase between 880 and 980 K, which is consistent with the available Al-rich range AlMnSi phase diagram. However, the residual low-intensity x-ray peaks in this temperature range could not be indexed on the basis of β(MnSi) or o-Al_6Mn phases, as would suggest the equilibrium phase diagram. Above 1000 K, the $\rho(T)$ behaviour tends to the resistivity of the β-Al_9Mn_3Si phase as indicated

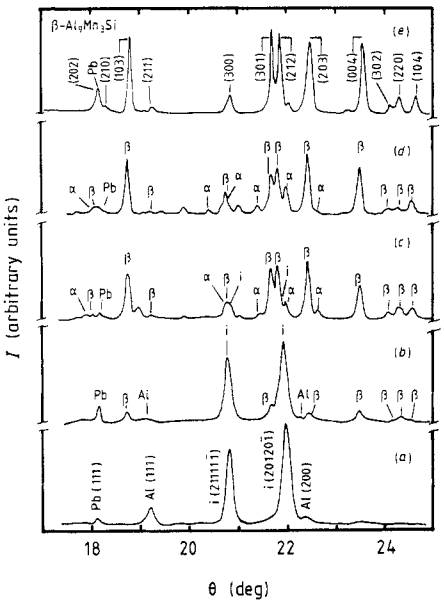

Figure 11. X-ray diagram for $Al_{75}Mn_{20}Si_5$: (*a*) as-quenched; annealed up to (*b*) 790 K, (*c*) 880 K, (*d*) 910 K, (*e*) 1000 K. The peaks labelled 'Pb' correspond to the lead holder.

by the x-ray diagram which is indexed with the β-phase alone. No Al phase is detected by x-ray diffraction, indicating a β-phase concentration range.

To complete this study we performed high-temperature measurements on the crystalline AlMnSi phases and on the decagonal 'T' phase. However, we note here the differences between the two quasi-crystalline systems (AlMn and AlMnSi) which up to now have not been distinguished by structural models. Our low-temperature resistivity, specific heat and magnetic susceptibility measurements [4] also recently underlined this point, and raised the question of possible differences in the i-phase in both alloys (Mn concentration, local environments, nature of disorder), or of the exact role of Si more often assimilated to Al.

6. Conclusion

Resistivity, DSC and x-ray diffraction studies were combined in the temperature range 300–1000 K to follow the irreversible structural transformations of icosahedral AlMn(Si) melt-spun ribbons. In $Al_{86}Mn_{14}$ and $Al_{90}Mn_{10}$ the analysis of our resistivity data within a two-phase model allowed us to estimate the resistivity for the i-phase to be 150–200 $\mu\Omega$ cm. The analysis of the DSC and x-ray spectra leads to a crystallisation of both the icosahedral and residual intergranular **Al**Mn solid solution into o-Al_6Mn preceded by a 'relaxation' phenomenon. The analysis of the amplitude and the temperature dependence of resistivity are well understood by taking into account the different phase contributions to resistivity during the transformation: the initial decrease in $\rho(T)$ for $Al_{86}Mn_{14}$ is attributed to a relaxation in the i-phase and to the beginning of o-Al_6Mn crystallisation; the following steep rise in $\rho(T)$ is ascribed to the rapid decrease of the volume fraction of the low-resistivity AlMn solid solution. In $Al_{90}Mn_{10}$, the same

description accounts for the observed amplitude and temperature variations of resistivity.

The $Al_{75}Mn_{20}Si_5$ sample, which is an almost pure i-phase, reveals a more complex crystallisation behaviour involving several intermediate phases. Finally it crystallises into the single β-Al_9Mn_3Si phase. Better stability of the AlMnSi i-phase, as compared to AlMn i-phase both in temperature (~700 K and ~600 K, respectively) and against decagonal 'T' phase formation implies possible structural or electronic differences.

Acknowledgment

One of us (CB) is grateful to CEA for financial support.

References

[1] Shechtman D, Blech I, Gratias D and Cahn J 1984 *Phys. Rev. Lett.* **53** 1951
[2] Henley C L 1987 *Comment. Cond. Matt. Phys.* **13** 59
[3] Pavuna D, Berger C, Cyrot-Lackmann F, Germi P and Pasturel A 1986 *Solid State Commun.* **59** 11
[4] Lasjaunias J C, Tholence J L, Berger C and Pavuna D 1987 *Solid State Commun.* **64** 425
Berger C, Lasjaunias J C, Tholence J L, Pavuna D and Germi P 1988 *Phys. Rev.* B **37** 6525
[5] Chen H S and Chen C H 1986 *Phys. Rev.* B **33** 668
[6] Yu-Zhang K, Harmelin M, Quivy A, Calvayrac Y, Bigot J and Portier R 1988 *Mater. Sci. Eng.* **99** 385
[7] Kimura K, Hashimoto T, Suzuki K, Nagayama K, Inoue H and Takeuchi S 1986 *J. Phys. Soc. Japan* **55** 534
[8] Pannetier J, Dubois J M, Janot Ch and Bilde A 1987 *Phil. Mag.* B **55** 435
[9] Baxter D V, Schulz R, Carpenter G J C and Strom Olsen J O 1988 *Mater. Sci. Eng.* **99** 399
[10] Samuel F, Samuel A, de Jonckère A and Gerin F 1986 *Met. Trans.* A **17** 1671
[11] Koster U and Schumacher B 1988 *Mater. Sci. Eng.* **99** 417
[12] Pavuna D 1981 *J. Mater. Sci.* **16** 2419
[13] Cahn J W, Shechtman D and Gratias D 1986 *J. Mater. Res.* **1** 13
[14] Jones H 1982 *J. Mater. Sci. Lett.* **1** 405
[15] Guyot P and Audier M 1985 *Phil. Mag.* B **52** L15
Shaefer R J, Bendersky L A and Biancaniello F S 1986 *J. Physique Coll. Suppl.* 7 **47** C3 311
[16] Hamzić A, Babić E and Leontić B 1986 *Mater. Sci. Eng.* **23** 271
[17] Rivier N and Zlatić V 1972 *J. Phys. F: Met. Phys.* **2** L87
[18] Yoshida K 1986 *Phil. Mag.* B **53** 55
[19] Landauer R 1952 *J. Appl. Phys.* **13** 779
[20] Chen H S 1978 *J. Non-Cryst. Solids* **27** 257
[21] Bhat S P, Ramachandran T R and Jena A K 1974 *J. Mater. Sci.* **9** 1759
[22] Mukhopadhyay N K, Ranganathan S and Chattopadhyay K 1987 *Phil. Mag. Lett.* **56** 121